PNAS
www.pnas.org

# Supplementary Information for

## The Amyloid Clearance Defect in ApoE4 Astrocytes is Reversed by Epigenetic Correction of Endosomal pH

Hari Prasad and Rajini Rao

Rajini Rao
Email: rrao@jhmi.edu

**This PDF file includes:**

Supplementary text
Figs. S1 to S8
References for SI reference citations



www.pnas.org/cgi/doi/10.1073/pnas.1801612115

## Supplementary Information Text

## Supplemental Information includes Extended Experimental Procedures and eight figures.

## Extended Experimental Procedures

### Antibodies and Reagents

Mouse monoclonal antibodies used were External epitope Anti-LRP1 (#ab20753, Abcam), Anti-HDAC4 (4A3) (#5392, Cell Signaling Technology), Anti-α-Tubulin (#T9026, Sigma), Anti-β-Actin (#A5441, Sigma), and Anti-GFP (4B10) (#2955, Cell Signaling Technology). Rabbit monoclonal antibodies used were Internal epitope Anti-LRP1 (#ab92544, Abcam), Anti-$Na^+/K^+$-ATPase (#3010, Cell Signaling Technology), Anti-Acetyl-Histone H3 (Lys14) (D4B9) (#7627, Cell Signaling Technology), and Anti-Acetyl-Histone H4 (Lys8) (#2594, Cell Signaling Technology). Specific rabbit polyclonal NHE6 antibody was raised against the C terminus of NHE6(1). Monensin (#M5273), Sodium valproate (#P4543), and Sodium butyrate (#B5887) were obtained from Sigma. Clioquinol (#130-26-7) was purchased from Calbiochem. HDAC inhibitors CI994(#A4102), MC1568(#A4094), Tubacin (#A4501), LBH589 (#A8178), TSA (#A8183), and SAHA (#A4084) were from ApexBio Technology.

### Cell Culture

Human ApoE isoform-expressing (ApoE3 and ApoE4) and $ApoE^{KO}$ astrocytes (gift from Dr. David M. Holtzman, Washington University, St. Louis) were maintained in DME-F12 (Invitrogen) supplemented with 10% fetal bovine serum (FBS) (Invitrogen) and 200μg/ml Geneticin/G418 (Corning Cellgro). ApoE3/3 (#AG04387) and ApoE4/4 (#AG10788) fibroblast cell lines were from Coriell Institute for Medical Research. Fibroblasts were grown in Eagle's MEM (Sigma) containing 10% FBS, non-essential amino acids (Quality Biological) and Glutamax (Invitrogen). ApoE genotyping was confirmed by sequencing analysis(2). Culture conditions were in a 5% $CO_2$ incubator at 37°C. Cell viability was measured using the trypan blue exclusion method.

### Plasmids and transfection

NHE6-GFP and NHE9-GFP were cloned into FUGW-lentiviral vector into the BamHI site. QuikChange Lightning site-directed mutagenesis kit (#21051, Agilent Technologies) was used to engineer L188P and G383D missense substitutions into NHE6. Resulting plasmids were confirmed by sequencing. Astrocytes were transfected using lentiviral packaging and expression.

### Bioinformatics and structural modeling

Mammalian gene expression datasets included in the study were GSE5281, GSE1297, GSE4757, GSE5281, GSE16759, E-MEXP-2280, and GSE15222. Gene Ontology (GO) enrichment analysis was performed using tools provided at the GO web site (http://www.geneontology.org). Pooled analysis was performed using the RevMan program (Nordic Cochrane Centre), as previously described(1). We constructed a structural model of the membrane domain of NHE6 based on the crystal structure of a distantly related *E. coli* bacterial ortholog, NhaA (1zcd), as previously described(3, 4). Evolutionary conservation scores were calculated using the Bayesian method using the Consurf web server (http://consurf.tau.ac.il/) that analyses the evolutionary pattern of the amino acids to reveal functionally important regions. The three-dimensional NHE6 model structure was colored by the new color-blind friendly evolutionary conservation scale(5). Consistent with the reliability of developed the NHE6 model structure, we observed preponderance of evolutionarily conserved residues within the core regions of the transporter.

**Transferrin, dextran and EGF uptake**

Steady state transferrin uptake was measured using flow cytometry and confocal microscopy, as we previously described(1, 3). Briefly, cells were rinsed and incubated in serum-free medium for 30min, to remove residual transferrin and then incubated with Alexa Fluor 633-Transferrin (#T23362, Thermo Fisher Scientific) (100 μg/ml) at 37°C for 60min. Transferrin uptake was stopped by placing the cells on ice. Excess transferrin was removed by washing with ice-cold serum-free DMEM and PBS, whereas bound transferrin was removed by 2x washing with ice-cold pH 5.0 PBS and pH 7.0 PBS. Cells were fixed with a solution of 4% paraformaldehyde for confocal imaging using the LSM 700 Confocal microscope (Zeiss), or trypsinized for flow cytometry analysis of ~10,000 cells in biological triplicates using the FACSAria instrument (BD Biosciences). Dextran uptake was quantified using flow cytometry following 12h of incubation with Alexa Fluor 647-Dextran (#D22914, Thermo Fisher Scientific) (10 μg/ml) at 37°C. Similarly, EGF uptake was quantified using flow cytometry following 1h of incubation with Alexa Fluor 488-EGF (#E13345, Thermo Fisher Scientific) (100 ng/ml) at 37°C. Unstained cells without any exposure to fluorescently-labeled cargo were used as a control for background fluorescence.

**Quantitative Real-time PCR**

mRNA was extracted from cell cultures using the RNeasy Mini kit (#74104, Qiagen) with DNaseI (#10104159001, Roche) treatment, following the manufacturer's instructions. Complementary DNA was synthesized using the high-Capacity RNA-to-cDNA Kit (#4387406, Applied Biosystems). Quantitative real-time PCR analysis was performed using the 7500 Real-Time PCR System (Applied Biosystems) using Taqman Fast universal PCR Master Mix (#4352042, Applied Biosystems). Taqman gene expression assay probes used in this study are: Mouse: NHE6, Mm00555445_m1; NHE9, Mm00626012_m1; NHE1, Mm00444270_m1; ATP6V0A1, Mm00444210_m1; LRP1, Mm00464608_m1, NF-L, Mm01315666_m1; TUBB3, Mm00727586_s1; ACTB, Mm02619580_g1; and GAPDH, Mm99999915_g1. Human: NHE6, Hs00234723_m1; NHE9, Hs00543518_m1; ATP6V0A1, Hs00989334_m1; GAPDH, Hs02786624_g1. The Ct (cycle threshold) values were used for all experiments and were first normalized to endogenous control levels by calculating the ΔCt for each sample. Values were then analyzed relative to control, to generate a ΔΔCt value. Fold change was obtained using the equation, expression fold change=$2^{-\Delta\Delta Ct}$. Each experiment was repeated three times independently.

**Immunofluorescence**

Cultured cells on polyornithine-coated coverslips were pre-extracted with PHEM buffer (60mM PIPES, 25mM HEPES, 10mM EGTA and 2mM $MgCl_2$, pH 6.8) containing 0.025% saponin for 2 min, then washed twice for 2 min with PHEM buffer containing 0.025% saponin and 8% sucrose. The cells were fixed with a solution of 4% paraformaldehyde (Electron Microscopy Sciences) and 8% sucrose in PBS for 30min at room temperature and blocked with a solution of 1% BSA and 0.025% saponin in PBS for 1hour. Cells were stained for primary antibodies and Alexa Fluor-conjugated secondary antibodies, DAPI-stained, and mounted onto slides using Dako fluorescent mounting medium and were imaged using a LSM 700 Confocal microscope (Zeiss). Slides were imaged with a ×63 oil immersion objective. Expression of empty GFP vector and NHE6-GFP was detected using the GFP fluorescence. Fractional colocalization was determined from the Pearson's correlation coefficient, using the JACoP ImageJ plugin that measures the direct overlap of pixels in the confocal section, and represented it as mean ± S.E.

**Western blot and surface biotinylation**

Cells were lysed using 1% Nonidet P-40 (Sigma) supplemented with protease inhibitor cocktail (Roche). Cells were sonicated and then centrifuged for 15 min at 14,000 rpm at 4°C. Protein concentration was determined using the BCA assay. Surface biotinylation was performed using Pierce Cell Surface Protein Isolation Kit (#89881, Thermo Fisher Scientific), as per manufacturer's

instructions. Equal amounts of total protein or cell surface protein were separated by polyacrylamide gel (NuPAGE Novex) under reducing conditions and then electrophoretically transferred onto nitrocellulose membranes (Bio-Rad). Ponceau stain or GelCode blue stain (#24590, Thermo Fisher Scientific) was used to confirm protein transfer. The membranes were treated with the blocking buffer containing 5% milk, followed by overnight incubation with primary antibodies and 1h incubation with HRP-conjugated secondary antibodies (GE Healthcare). SuperSignal West Pico substrate was used for detection. Amersham Imager 600 system was used to capture images and densitometric quantification was done using ImageJ software.

**Endosomal pH measurement**

Endosomal pH was measured using flow cytometry, as we previously described(1, 3). Briefly, cells were rinsed and incubated in serum-free medium for 30min, to remove residual transferrin and then incubated with pH-sensitive FITC-Transferrin (#T2871, Thermo Fisher Scientific) (75 μg/ml) together with pH non-sensitive Alexafluor 633-Transferrin (#T23362, Thermo Fisher Scientific) (25 μg/ml) at 37°C for 55min. For experiments with GFP tagged NHE6 (wild type and mutants), we used pH-sensitive pHrodo Red-Transferrin (#P35376, Thermo Fisher Scientific), to avoid spectral overlap. Transferrin uptake was stopped by placing cells on ice. Excess transferrin was removed by washing with ice-cold serum-free DMEM and PBS, whereas bound transferrin was removed by washing with ice-cold pH 5.0 PBS and pH 7.0 PBS. Cells were trypsinized and pH was determined by flow cytometry analysis of ~10,000 cells in biological triplicates using the FACSAria instrument (BD Biosciences). Cells were gated on a forward scatter and side scatter. Live single cells were further sorted to obtain cells that have internalized both pH sensitive and pH non-sensitive fluorophores. A four-point calibration curve with different pH values (4.5, 5.5, 6.5 and 7.5) was generated using Intracellular pH Calibration Buffer Kit (#P35379, Thermo Fisher Scientific) in the presence of 10μM $K^+/H^+$ ionophore nigericin and 10μM $K^+$ ionophore valinomycin.

**Lysosomal pH measurement**

Lysosomal pH was measured as previously described, with modifications(6, 7). Briefly, cells were incubated with pH-sensitive pHrodo-green-Dextran (#P35368, Thermo Fisher Scientific) (5 μg/ml) together with pH non-sensitive Alexa Fluor 647-Dextran (#D22914, Thermo Fisher Scientific) (10 μg/ml) for 12 hours, washed then chased in dye free media for additional 6 hours. For experiments with GFP tagged NHE6, we used pH-sensitive pHrodo Red-Dextran (#P10361, Thermo Fisher Scientific), to avoid spectral overlap. Cells were trypsinized and pH was determined by flow cytometry analysis of ~10,000 cells in biological triplicates using the FACSAria instrument (BD Biosciences). Cells were gated on a forward scatter and side scatter. Live single cells were further sorted to obtain cells that have internalized both pH sensitive and pH non-sensitive fluorophores. A four-point calibration curve with different pH values (3.5, 4.5, 5.5 and 6.5) was generated in the presence of 10μM $K^+/H^+$ ionophore nigericin and 10μM $K^+$ ionophore valinomycin.

**Cytoplasmic pH measurement**

Cytoplasmic pH was measured using flow cytometry, as previously described(8, 9). Briefly, cells were washed and incubated with 1μM BCECF-AM (Thermo Fisher Scientific) for 30min. Cells were trypsinized and pH was determined using flow cytometry analysis of ~10,000 cells in biological triplicates using the FACSAria instrument (BD Biosciences) by excitation at 488nm and emissions filtered through 530 (±15) nm (pH-sensitive green fluorescence) and 616 (±12) nm (pH non-sensitive red fluorescence) filters. A pH calibration curve was generated by preloading cells with 1μM BCECF-AM for 30min followed by incubation in a 'high $K^+$' HEPES buffer (25mM HEPES, 145mM KCl, 0.8mM $MgCl_2$, 1.8mM $CaCl_2$, 5.5mM glucose) with pH adjusted to different values (6.6, 7.0, 7.4 and 7.8), and used to prepare a four-point calibration curve in the presence of 10μM $K^+/H^+$ ionophore nigericin.

**Baculovirus Transduction**

For subcellular localization of endocytosed Aβ, we used CellLight-Bacmam 2.0 transduction technology (Molecular probes). Culture medium from ApoE3 astrocyte culture was aspirated, and fresh medium containing CellLight RFP-Bacmam 2.0 reagent targeting representative markers of early endosome (#C10587, Rab5) or late endosome (#C10589, Rab7), or lysosome (#C10504, Lamp1) was added to reach a final concentration of 30 particles per cell, as suggested by the manufacturer's instructions. Four hours after transduction 100 nM fluorescently-labeled HiLyte Fluor 647-Aβ (#AS-64161, AnaSpec) was added to the media and cultured for an additional 12 hours. Cells were fixed with a solution of 4% paraformaldehyde, DAPI-stained, and mounted onto slides to determine subcellular localization of Aβ by confocal imaging.

**LRP1 surface labeling**

LRP1 surface labeling was performed by immunofluorescence and flow cytometry using a mouse monoclonal antibody against an extracellular epitope of LRP1 (#ab20753, Abcam). For immunofluorescence, live cells were incubated with primary antibody on ice for 1 hour. Cells were then fixed, incubated with secondary antibody, DAPI stained and mounted onto slides to quantify surface LRP1 levels by confocal microscopy. For flow cytometry, live cells were dissociated non-enzymatically with 0.2% EDTA (in PBS) followed by gentle scraping and filtering through a cell strainer and incubated with primary antibody for 30 minutes on ice. Cells were then washed, incubated with secondary antibody, and subjected to flow cytometry analysis of ~5,000 cells in biological triplicates.

**LRP1 internalization**

LRP1 internalization was quantified as previously described, with modifications(10). ApoE3 and ApoE4 astrocytes were placed on ice and washed once with DME-F12/ 5% FBS/ 30 mM HEPES (used for all staining and subsequent wash steps). Cells were labeled with antibody against an extracellular epitope of LRP1 for 1 h on ice and washed twice to remove unbound antibody. Cells were either incubated at 4 °C or at 37 °C for 10min to allow LRP1 internalization and then placed immediately on ice to stop further endocytosis. Cells were washed twice, and remaining surface-bound anti-LRP1 antibody was stained with an Alexa Fluor 633-conjugated secondary antibody for 30 min on ice. Samples were washed twice, collected, and analyzed by flow cytometry using the FACSCalibur instrument (BD Biosciences).

**Aβ surface-binding assay**

Ligand surface-binding assay was performed as we previously described, with modifications(8). Cells on coverslips were rinsed and incubated in serum-free medium for 30min and then exposed to 100 nM fluorescently-labeled HiLyte Fluor 647-Aβ (#AS-64161, AnaSpec) in 1% BSA solution on ice for 10min, followed by subsequent washes with PBS at pH 7.0. Cells were then fixed, DAPI stained and mounted onto slides to quantify Aβ surface-binding by confocal microscopy.

**HDAC nuclear translocation**

For quantifying HDAC4 nuclear translation, we immunostained cells using a mouse monoclonal antibody against HDAC4 (#5392, Cell Signaling Technology) and confocal images were analyzed to measure colocalization between HDAC4 and nuclear stain DAPI. Next, we performed nuclear fractionation of cultured cells using Nuclei isolation kit (#NUC-101, Sigma), as per manufacturer's instructions. Protein concentration was determined using the BCA assay. Protein from nuclear lysates was resolved using SDS-PAGE and transferred to nitrocellulose membranes. The membranes were then probed with anti-HDAC4 antibody to detect HDAC4 in the nuclear fraction.

Fig. S1

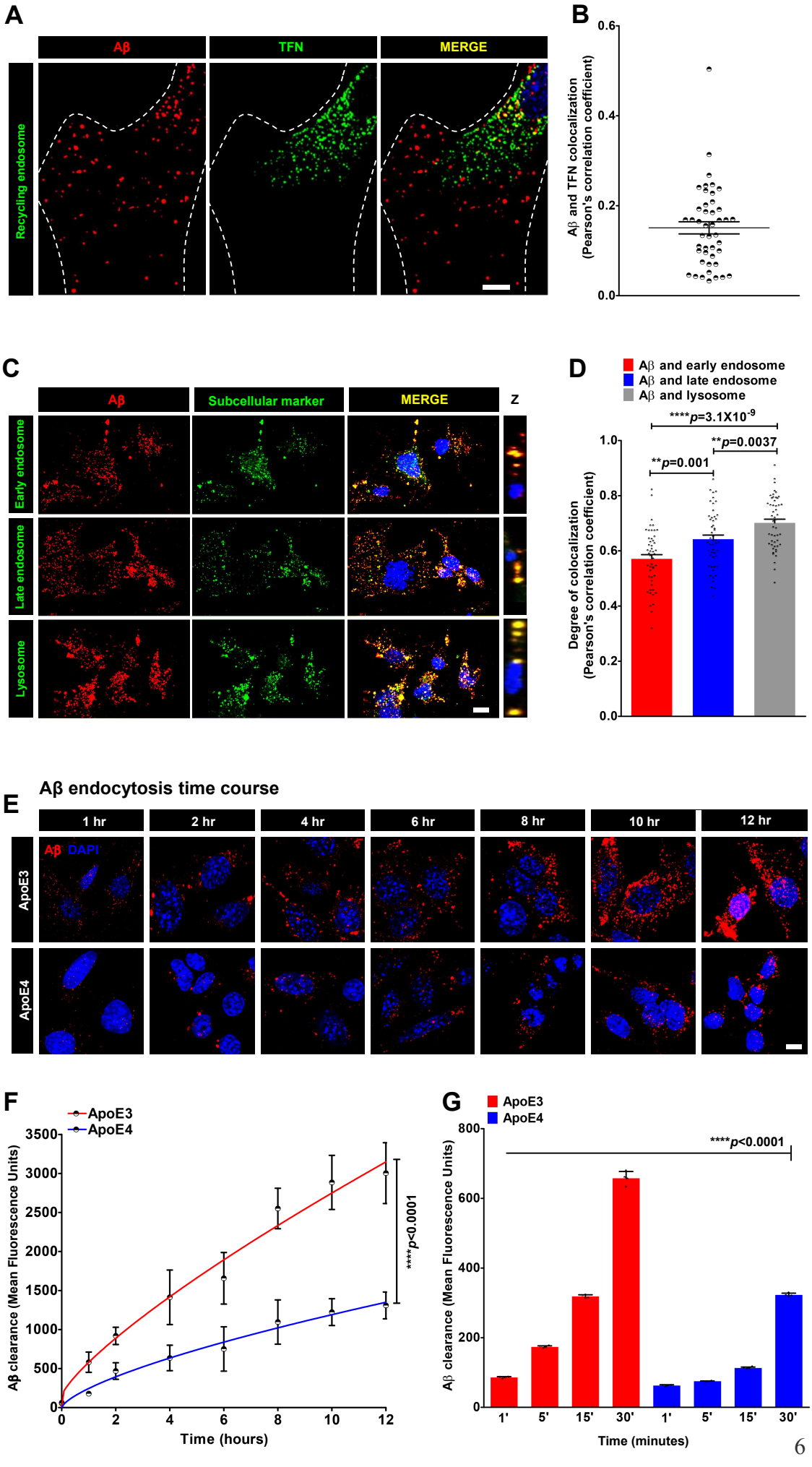
A
Aβ
TFN
MERGE
Recycling endosome
B
Aβ and TFN colocalization (Pearson's correlation coefficient)
0.0
0.2
0.4
0.6
C
Aβ
Subcellular marker
MERGE
Z
Early endosome
Late endosome
Lysosome
D
Aβ and early endosome
Aβ and late endosome
Aβ and lysosome
****p=3.1X10-9
**p=0.0037
**p=0.001
Degree of colocalization (Pearson's correlation coefficient)
0.0
0.2
0.4
0.6
0.8
1.0
E
Aβ endocytosis time course
1 hr
2 hr
4 hr
6 hr
8 hr
10 hr
12 hr
Aβ DAPI
ApoE3
ApoE4
F
ApoE3
ApoE4
Aβ clearance (Mean Fluorescence Units)
0
500
1000
1500
2000
2500
3000
3500
0
2
4
6
8
10
12
Time (hours)
****p<0.0001
G
ApoE3
ApoE4
****p<0.0001
Aβ clearance (Mean Fluorescence Units)
0
200
400
600
800
1'
5'
15'
30'
1'
5'
15'
30'
Time (minutes)

**Fig. S1. ApoE isotype-specific differences in Aβ clearance. Related to Fig. 1.**

(A-B) Representative micrographs (A) and quantification using Pearson's correlation (B) determining fractional colocalization of Aβ (red) with transferrin (TFN) (green) in DAPI-(blue) stained ApoE3 astrocytes, following 60 minutes of uptake. Note poor colocalization, as evident in the merge and orthogonal slices (Z) with fewer yellow puncta (Pearson's correlation: 0.16±0.09; $n$=45), suggesting that a significant pool of internalized Aβ escapes recycling endosomes. (C-D). Micrographs (C) and quantification using Pearson's correlation (D) determining fractional colocalization of Aβ (red) with representative early endosomal (Rab5), late endosomal (Rab7) and lysosomal (Lamp1) compartment markers (green) in DAPI-(blue) stained ApoE3 astrocytes following 12h of uptake. Colocalization is evident in the merge and orthogonal slices (Z) as yellow puncta. (E-F). Time course of Aβ accumulation in ApoE3 and ApoE4 astrocytes by confocal microscopy. Representative images are shown (E) and mean fluorescence ± s.e. was plotted (F). ApoE4 cells show a reduced rate and total Aβ accumulation, relative to ApoE3 astrocytes (****$p$<0.0001; Student's $t$-test). (G) Quantification of Aβ clearance from FACS analysis of ApoE3 and ApoE4 cells at very early time points between 1-30 min. Note significantly lower cell-associated Aβ in ApoE4 relative to ApoE3 at all time points (****$p$<0.0001; $n$=3; Student's $t$-test). Scale bars, 10μm.

Fig. S2

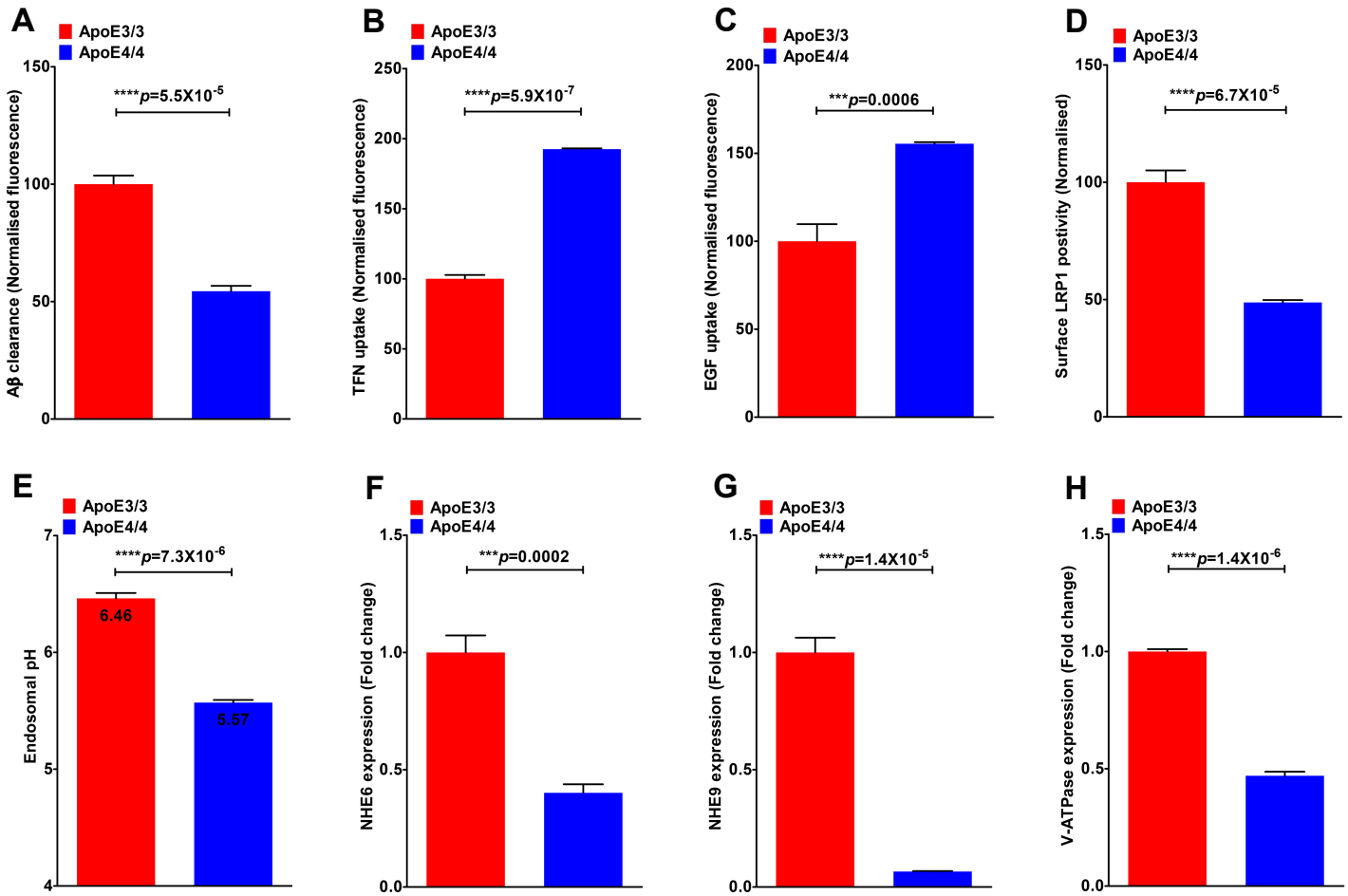
A
ApoE3/3
ApoE4/4
****p=5.5X10-5
Aβ clearance (Normalised fluorescence)
150
100
50
0
B
ApoE3/3
ApoE4/4
****p=5.9X10-7
TFN uptake (Normalised fluorescence)
250
200
150
100
50
0
C
ApoE3/3
ApoE4/4
***p=0.0006
EGF uptake (Normalised fluorescence)
200
150
100
50
0
D
ApoE3/3
ApoE4/4
****p=6.7X10-5
Surface LRP1 postivity (Normalised)
150
100
50
0
E
ApoE3/3
ApoE4/4
****p=7.3X10-6
Endosomal pH
7
6
5
4
6.46
5.57
F
ApoE3/3
ApoE4/4
***p=0.0002
NHE6 expression (Fold change)
1.5
1.0
0.5
0.0
G
ApoE3/3
ApoE4/4
****p=1.4X10-5
NHE9 expression (Fold change)
1.5
1.0
0.5
0.0
H
ApoE3/3
ApoE4/4
****p=1.4X10-6
V-ATPase expression (Fold change)
1.5
1.0
0.5
0.0

**Fig. S2. ApoE genotyped human fibroblasts recapitulate findings from mouse astrocytes. Related to Fig. 1-4.**

A. Quantification of FACS analysis showing ~46% reduction in Aβ uptake in AD patient derived ApoE4/4 primary fibroblasts, relative to age matched ApoE3/3 control (****$p$=5.5X10$^{-5}$; $n$=3; Student's $t$-test). B. Quantification of FACS analysis showing ~1.93-fold increase in transferrin (TFN) uptake in ApoE4/4 fibroblasts, relative to ApoE3/3 control (****$p$=5.9X10$^{-7}$; $n$=3; Student's $t$-test). C. Quantification of FACS analysis showing ~1.56-fold increase in epidermal growth factor (EGF) uptake in ApoE4/4 fibroblasts, relative to ApoE3/3 control (***$p$=0.0006; $n$=3; Student's $t$-test). D. Fraction of LRP1 positive cells quantified following surface antibody labeling and FACS analysis of live, non-permeabilized cells in biological triplicates. Note ~51% lower surface LRP1 positivity in ApoE4/4 fibroblasts relative to ApoE3/3 control (****$p$=6.7X10$^{-5}$; $n$=3; Student's $t$-test). E. Hyperacidification of endosomal pH documented in ApoE4/4 fibroblasts, relative to ApoE3/3 control (~0.89 pH unit lower; ****$p$=7.3X10$^{-6}$; $n$=3; Student's $t$-test). (F-H). Quantitative PCR (qPCR) analysis showing significant downregulation of NHE6 (***p=0.0002; $n$=3; Student's $t$-test; F), NHE9 (****$p$=1.4X10$^{-5}$; $n$=3; Student's $t$-test; G), and V-ATPase subunit V0a1 (****$p$=1.4X10$^{-6}$; $n$=3; Student's $t$-test; H) in ApoE4/4 fibroblasts, relative to ApoE3/3 control.

Fig. S3

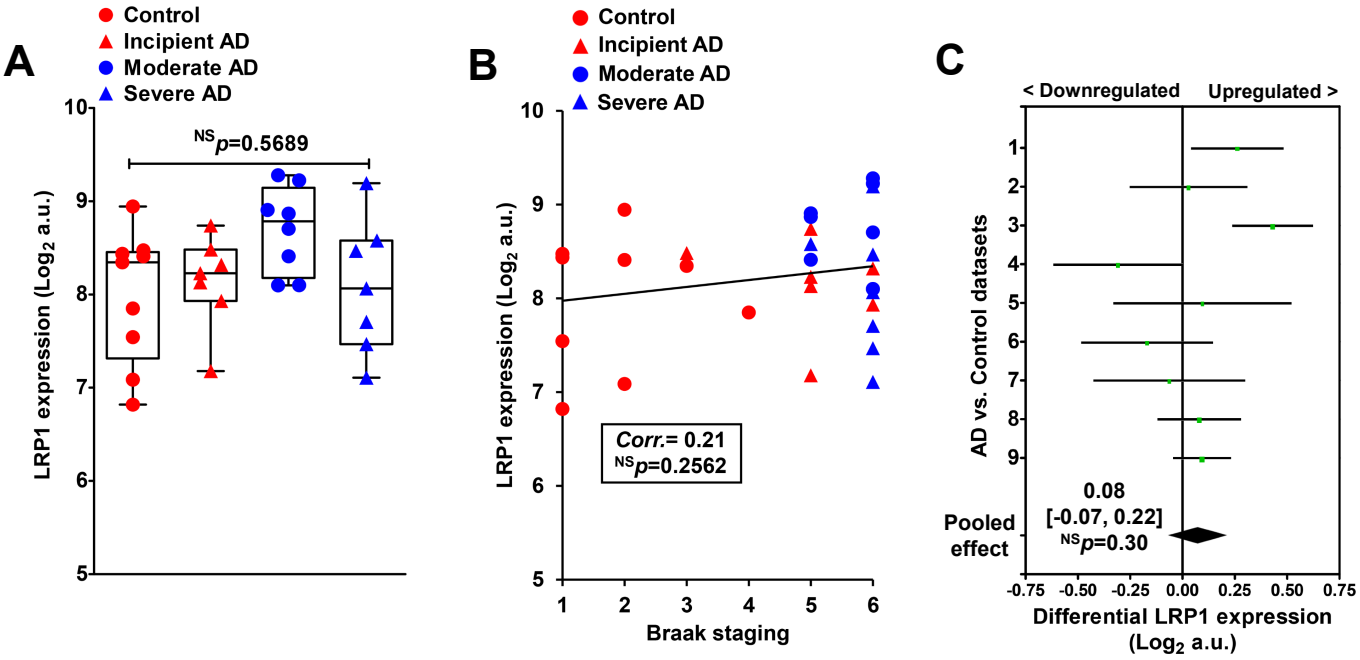


**D**

| Data set | Brain area | Ctrl | AD | Differential LRP1 expression [95% CI]* | Weight | *p*-value |
|---|---|---|---|---|---|---|
| 1 | Superior frontal gyrus | 9 | 22 | 0.26 [0.04, 0.48] | 12.6% | 0.02 |
| 2 | Parietal lobe | 4 | 4 | 0.03 [-0.25, 0.31] | 10.6% | 0.84 |
| 3 | Primary visual cortex | 12 | 17 | 0.43 [0.24, 0.62] | 13.6% | *p*<0.0001 |
| 4 | Middle temporal gyrus | 12 | 15 | -0.31 [-0.62, 0.00] | 9.7% | 0.05 |
| 5 | Middle temporal gyrus | 5 | 7 | 0.10 [-0.33, 0.52] | 6.9% | 0.66 |
| 6 | Entorhinal cortex | 12 | 10 | -0.17 [-0.48, 0.15] | 9.6% | 0.3 |
| 7 | Entorhinal cortex | 8 | 9 | -0.06 [-0.43, 0.30] | 8.3% | 0.74 |
| 8 | Posterior cingulate cortex | 13 | 9 | 0.08 [-0.12, 0.28] | 13.3% | 0.43 |
| 9 | Hippocampus | 12 | 10 | 0.09 [-0.05, 0.23] | 15.4% | 0.19 |
| | **Pooled effect** | **87** | **103** | **0.08 [-0.07, 0.22]** | **100.0%** | **0.30** |

*Random effects model (Log$_2$ a.u.)

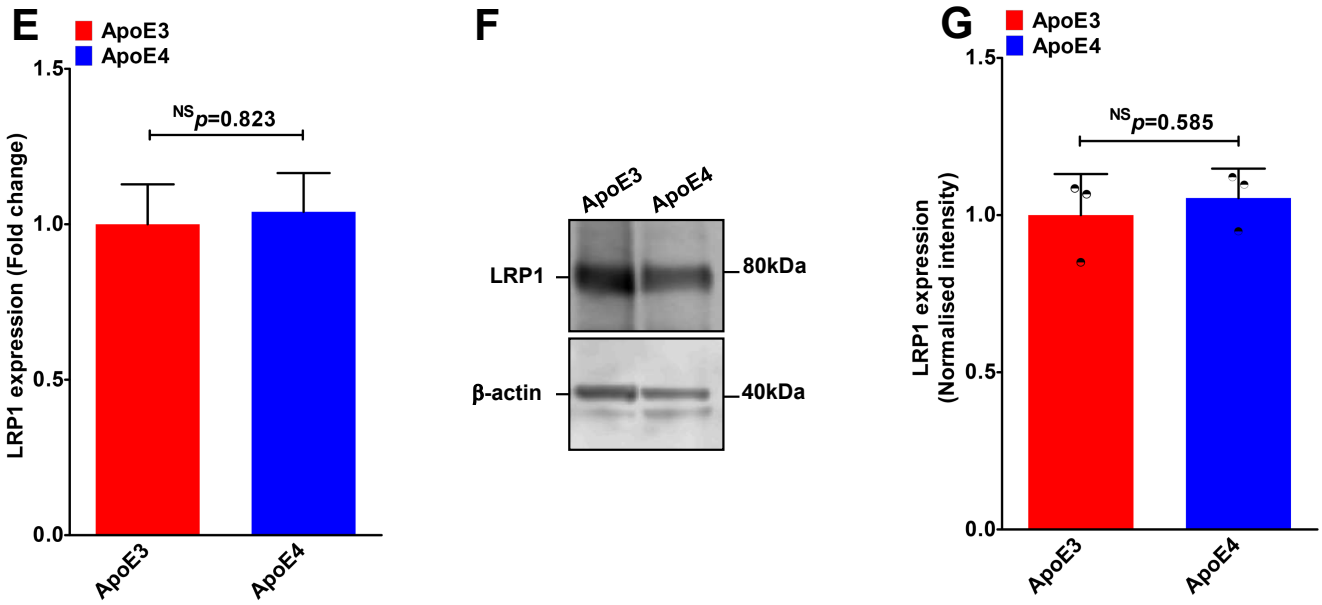

**Fig. S3. LRP1 transcript and total protein levels in ApoE isotypes. Related to Fig. 2.**

A. Box and whisker plots of hippocampal LRP1 gene expression across control and clinical stages of ($p$=0.569; $n$=31; ANOVA). B. Expression plot of LRP1 with post-mortem brain pathology assessed *via* Braak staging scores across all 31 subjects, regardless of diagnosis. Scores on the Braak staging range from 0 to 6, with higher scores indicate worse neuropathology. No correlation was observed for LRP1 levels with Braak stage (Pearson correlation coefficient=0.21; $n$=31; $p$=0.2562). Black line depicts linear fit. (C-D). Forest plot (C) and quantification (D) of differential LRP1 expression between AD and control (Ctrl) data sets and pooled average, represented as mean difference and 95% confidence interval (CI) of log base 2 expression, were obtained as described under "Experimental Methods." (Black diamond/pooled average=0.08; 95% CI= −0.07, 0.22; control, $n$=87; AD patients, $n$=103; $p$=0.30). E. LRP1 gene expression showing no significant difference between ApoE3 and ApoE4 astrocytes ($p$=0.823; Student's $t$-test). (F-G). Representative Western blot (F) and quantification of three biological replicates (G) showing total LRP1 protein expression normalized to β-actin levels between ApoE3 and ApoE4 astrocytes ($p$=0.585; $n$=3; Student's $t$-test). NS, Not significant.

Fig. S4

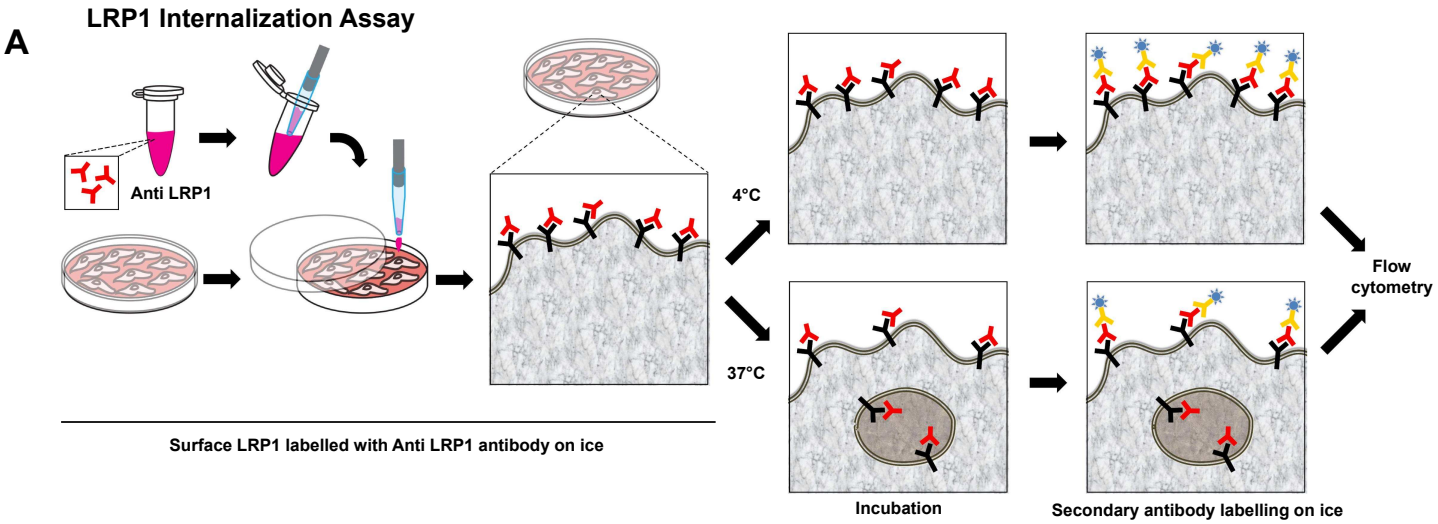
A
LRP1 Internalization Assay
Anti LRP1
4°C
37°C
Flow cytometry
Surface LRP1 labelled with Anti LRP1 antibody on ice
Incubation
Secondary antibody labelling on ice

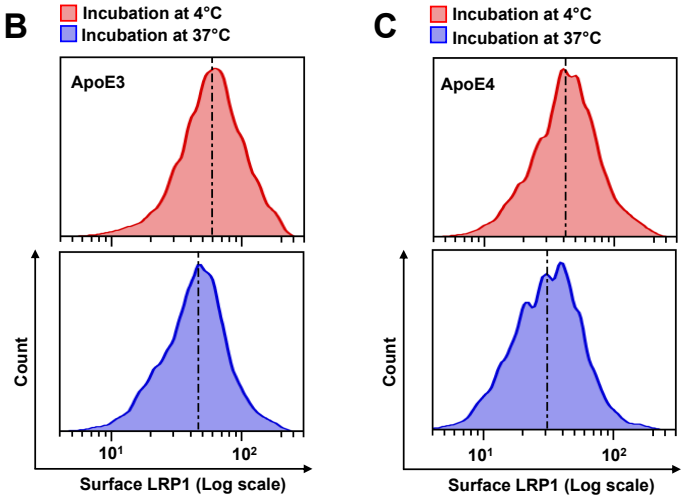
B
Incubation at 4°C
Incubation at 37°C
ApoE3
Count
$10^1$
$10^2$
Surface LRP1 (Log scale)


C
Incubation at 4°C
Incubation at 37°C
ApoE4
Count
$10^1$
$10^2$
Surface LRP1 (Log scale)

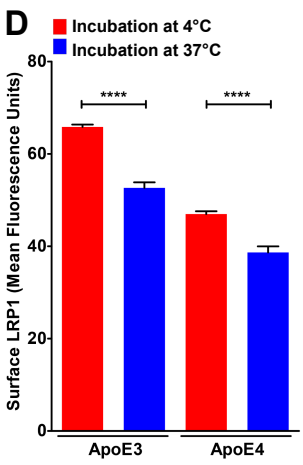
D
Incubation at 4°C
Incubation at 37°C
Surface LRP1 (Mean Fluorescence Units)
80
60
40
20
0
****
****
ApoE3
ApoE4

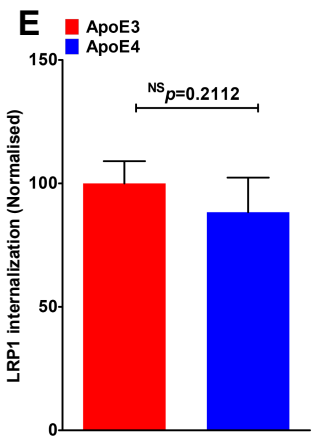
E
ApoE3
ApoE4
LRP1 internalization (Normalised)
150
100
50
0
NS p=0.2112

**Fig. S4. LRP1 internalization assay in ApoE3 and ApoE4 astrocytes. Related to Fig. 2.**

A. LRP1 internalization assay. ApoE3 and ApoE4 astrocytes were labeled with an antibody against an extracellular epitope of LRP1 on ice. After washing off unbound antibody, cells were either incubated at 4 °C or at 37 °C for 10min to allow LRP1 internalization. Remaining cell surface antibody-labeled LRP1 was detected with an Alexa Fluor 633-conjugated secondary antibody on ice and analyzed by flow cytometry. (B-C). Representative FACS histograms for ApoE3 (B) and ApoE4 (C) astrocytes depicting surface LRP1 staining following incubations at 4 °C (top panel, red) and 37 °C (bottom panel, blue). x-axis of the FACS histogram depicts LRP1 staining in logarithmic scale and vertical dashed line represents median fluorescence intensity. D. Quantification of mean fluorescence intensity of biological triplicates showing reduction in LRP1 staining with incubation at 37 °C, relative to incubation at 4 °C, due to LRP1 internalization (****$p$<0.0001; $n$=3; Student's $t$-test). Note lower LRP1 staining in ApoE4 astrocytes, relative to ApoE3, due to reduced surface expression. E. No difference in LRP1 internalization was observed between ApoE3 and ApoE4 astrocytes ($p$=0.2112; $n$=3; Student's $t$-test). NS, Not significant.

Fig. S5

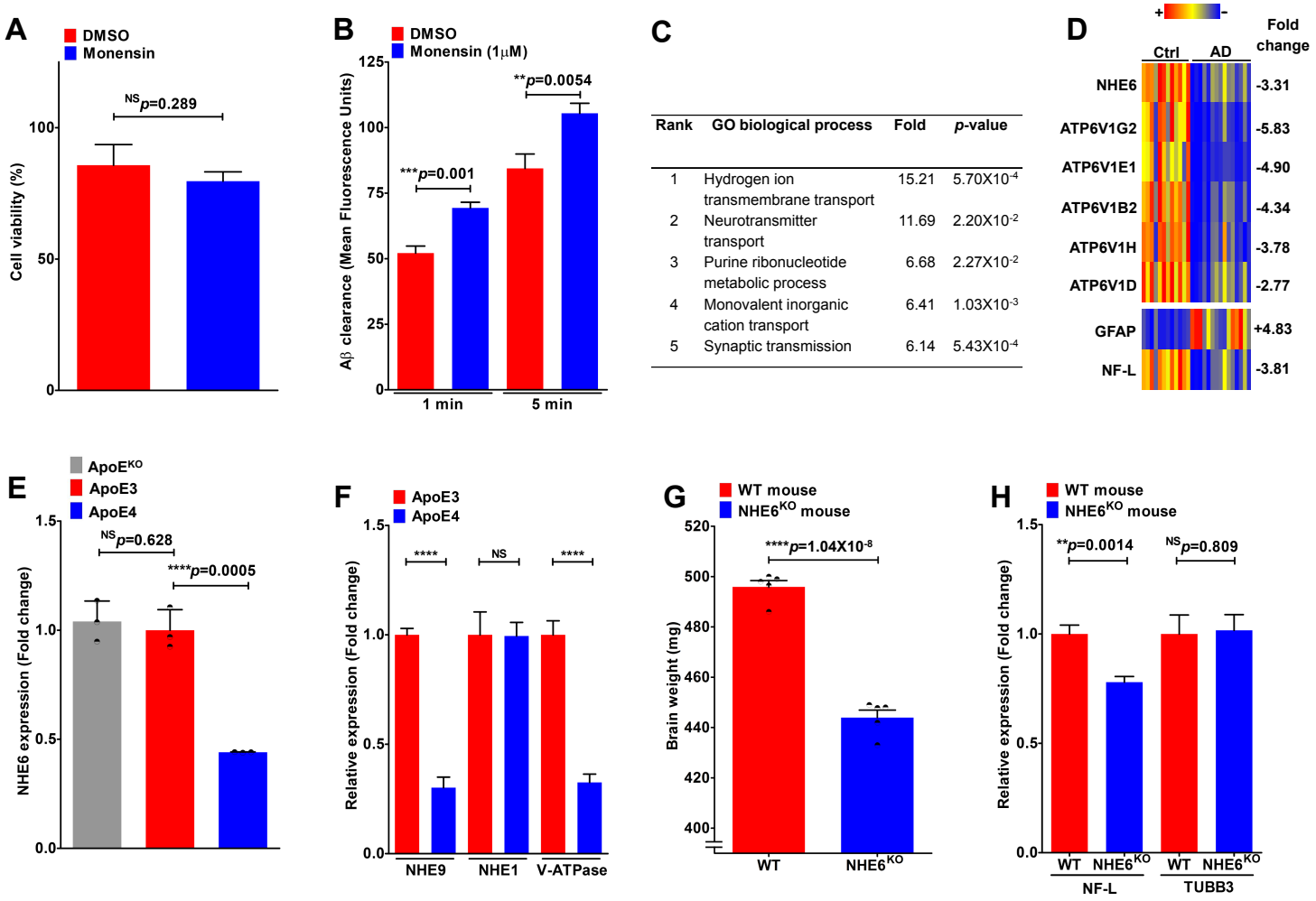


| Rank | GO biological process | Fold | *p*-value |
|---|---|---|---|
| 1 | Hydrogen ion transmembrane transport | 15.21 | $5.70X10^{-4}$ |
| 2 | Neurotransmitter transport | 11.69 | $2.20X10^{-2}$ |
| 3 | Purine ribonucleotide metabolic process | 6.68 | $2.27X10^{-2}$ |
| 4 | Monovalent inorganic cation transport | 6.41 | $1.03X10^{-3}$ |
| 5 | Synaptic transmission | 6.14 | $5.43X10^{-4}$ |

**Fig. S5. Genes regulating endolysosomal pH are dysregulated in Alzheimer's disease brains. Related to Fig. 3-4.**

A. Monensin treatment in ApoE4 astrocytes did not affect cell viability measured using trypan blue exclusion. B. Quantification of Aβ clearance from FACS analysis of ApoE4 cells at 1 and 5 min uptake following lower concentration monensin treatment (1μM, 8h), relative to DMSO control. (C-D). Gene ontology (GO) analysis of top-100 downregulated genes in post-mortem AD brains obtained as described under "Experimental Methods." Enrichment scores and p-values for top-5 GO biological process were shown (C). Note that genes involved in hydrogen ion transmembrane transport, including NHE6 and 5 V-ATPase subunits exhibited highest enrichment scores. Heatmaps of NHE6 and V-ATPase submits were shown, along with glial fibrillary acidic protein (GFAP) and neurofilament light chain (NF-L), for comparison (D). E. qPCR analysis of NHE6 transcript reveled significantly lower expression in ApoE4 astrocytes, relative to ApoE3 (~56% lower, ****$p$=0.0005, $n$=3; Student's $t$-test). No difference in NHE6 levels was observed between ApoE3 astrocytes and isogenic $ApoE^{KO}$ astrocytes ($p$=0.628; $n$=3; Student's $t$-test). F. qPCR analysis of NHE9 transcript reveled significantly lower expression in ApoE4 astrocytes, relative to ApoE3 (~70% lower; ****$p=2.7X10^{-5}$; $n$=3; Student's $t$-test). No changes in mRNA levels were observed for the closely related plasma membrane NHE1 isoform ($p$=0.946; $n$=3; Student's $t$-test). Note significantly lower mRNA levels for lysosomal V-ATPase V0a1 subunit in ApoE4 astrocytes, relative to ApoE3 (~67% lower; ****$p=9.7X10^{-5}$; $n$=3; Student's $t$-test). G. Consistent with clinical reports of microcephaly in Christianson syndrome patients, 7-month old hemizygous $NHE6^{KO}$ mice showed significantly lower brain weight, relative to wild-type mice. H. qPCR analysis revealed ~22% lower levels of neurofilament light chain (NF-L) characteristic of Alzheimer's pathology in 7- month old $NHE6^{KO}$ brains ($p$=0.0014; $n$=3; Student's $t$-test). No change in transcript levels of the neuronal protein TUBB3 was observed between WT and $NHE6^{KO}$ brains ($p$=0.809; $n$=3; Student's $t$-test). NS, Not significant.

Fig. S6

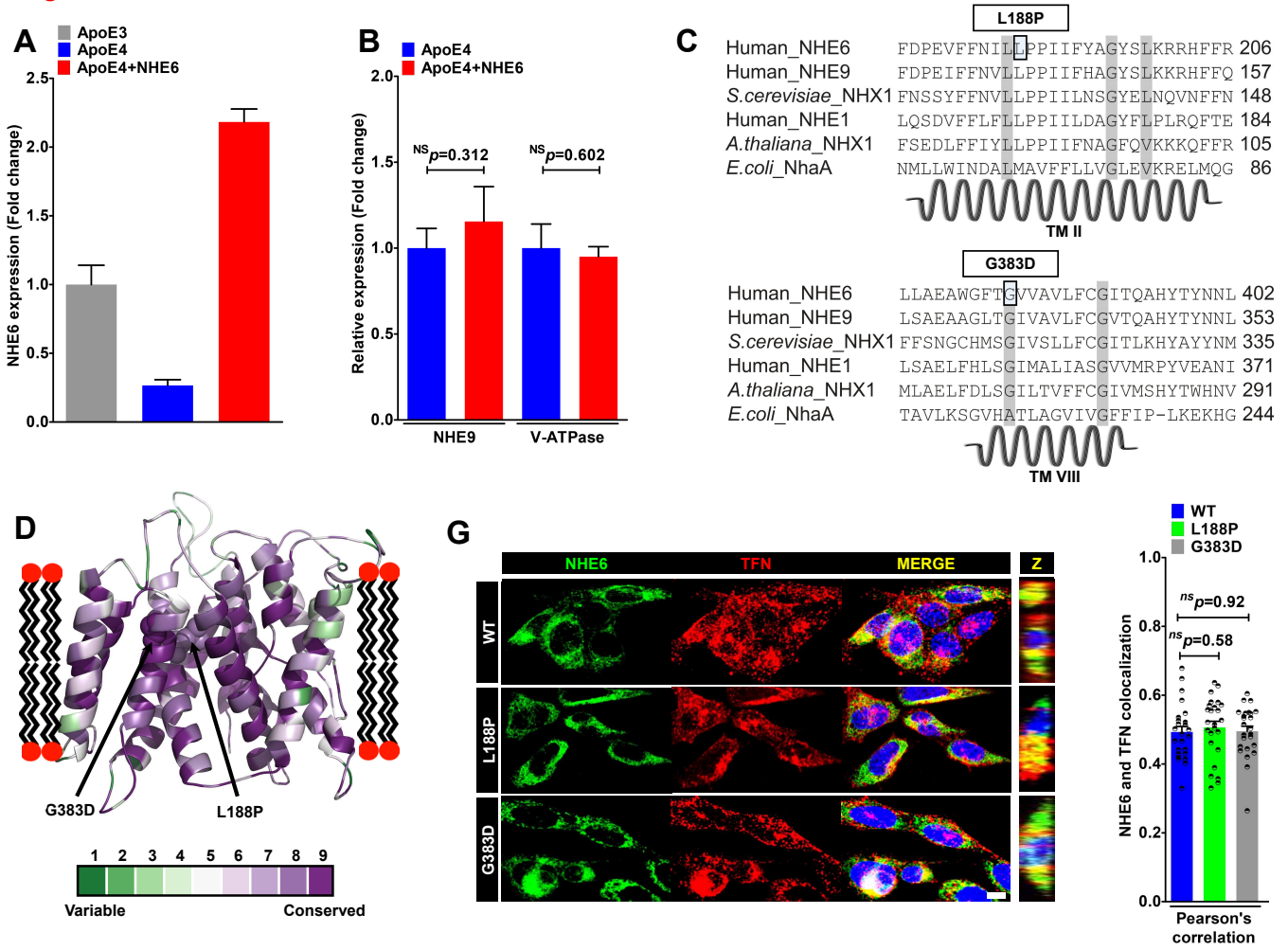
A
ApoE3
ApoE4
ApoE4+NHE6
NHE6 expression (Fold change)
B
ApoE4
ApoE4+NHE6
Relative expression (Fold change)
NS p=0.312
NS p=0.602
NHE9
V-ATPase
C
L188P
Human_NHE6 FDPEVFFNILLPPIIFYAGYSLKRRHFFR 206
Human_NHE9 FDPEIFFNVLLPPIIFHAGYSLKKRHFFQ 157
S.cerevisiae_NHX1 FNSSYFFNVLLPPIILNSGYELNQVNFFN 148
Human_NHE1 LQSDVFFLFLLPPIILDAGYFLPLRQFTE 184
A.thaliana_NHX1 FSEDLFFIYLLPPIIFNAGFQVKKKQFFR 105
E.coli_NhaA NMLLWINDALMAVFFLLVGLEVKRELMQG 86
TM II
G383D
Human_NHE6 LLAEAWGFTGVVAVLFCGITQAHYTYNNL 402
Human_NHE9 LSAEAAGLTGIVAVLFCGVTQAHYTYNNL 353
S.cerevisiae_NHX1 FFSNGCHMSGIVSLLFCGITLKHYAYYNM 335
Human_NHE1 LSAELFHLSGIMALIASGVVMRPYVEANI 371
A.thaliana_NHX1 MLAELFDLSGILTVFFCGIVMSHYTWHNV 291
E.coli_NhaA TAVLKSGVHATLAGVIVGFFIP-LKEKHG 244
TM VIII
D
G383D
L188P
1 2 3 4 5 6 7 8 9
Variable
Conserved
G
NHE6
TFN
MERGE
Z
WT
L188P
G383D
WT
L188P
G383D
NHE6 and TFN colocalization
NS p=0.92
NS p=0.58
Pearson's correlation
E
Mutation | Conservation score
L188P | 8
G383D | 9
Z
F
WT
L188P
G383D
kD
NHE6
76
52
Tubulin
52
H
Control
NHE6
L188P
G383D
Endosomal pH
NS p=0.94
NS p=0.72
** p=0.005
I
ApoE4
ApoE4+EV
ApoE4+NHE6
Lysosomal pH
NS p=0.905
NS p=0.20
J
Control
NHE6
L188P
G383D
Normalised Aβ clearance
NS p=0.698
NS p=0.087
*** p=0.0003
K
NHE9
TFN
DAPI
MERGE
Z
NHE9 and TFN colocalization Pearson's correlation coefficient
L
ApoE4
ApoE4+NHE9
Aβ clearance (Log scale)
Count
ApoE4
ApoE4+NHE9
Normalised Aβ clearance
NS p=0.155

**Fig. S6. Christianson syndrome mutants fail to correct Aβ clearance deficits in ApoE4 astrocytes. Related to Fig. 4.**

A. qPCR analysis showing the efficacy of overexpression of NHE6 in ApoE4 astrocytes. The data are plotted as average fold change of mRNA levels relative to ApoE3 astrocytes, with s.d. determined from triplicate measurements. B. qPCR analysis confirmed no concomitant changes in NHE9 ($p$=0.312; $n$=3; Student's $t$-test) and lysosomal V-ATPase V0a1 ($p$=0.602; $n$=3; Student's $t$-test) with lentiviral transduction of NHE6-GFP, relative to empty vector control. C. NHE6 and gene orthologue alignments showing residue conservation of Christianson syndrome (CS)-associated L188P (top) and G383D (bottom) substitutions in various species. (D-E) Side view of a model structure of the membrane domain of NHE6 based on the crystal structure of *E. coli* NhaA and colored according to the degree of ConSurf evolutionary conservation. Conservation color bar is shown at the bottom (D). L188P and G383D substitutions were mapped at highly conserved locations within the membrane-embedded transporter domain that corresponds to TM II and TM VIII in NhaA, respectively (E). F. Expression levels of NHE6 (WT and CS-associated variants). Immunoblot of total lysate from cells expressing NHE6-GFP, L188P-GFP, and G383D-GFP using an anti-GFP antibody. G. Fractional colocalization of NHE6 (WT and CS-associated variants) with endocytosed transferrin (TFN) following 1 h of uptake in ApoE4 astrocytes, quantified using Pearson's correlation shown on the right. Note that there are no significant differences in subcellular localization between GFP tagged variants, L188P and G383D, relative to WT NHE6. H. Expression of NHE6, but not CS-associated variants, in ApoE4 astrocytes with low endogenous NHE6 levels results in alkalization of endosomal pH. I. Lentiviral vector mediated expression of NHE6 in ApoE4 astrocytes does not alter lysosomal pH. Untransfected cells and empty vector transfected cells were used as controls. J. Quantitation of Aβ clearance from FACS analysis of 10,000 cells confirmed restoration of Aβ clearance over control (empty vector) in ApoE4 astrocytes expressing wild-type NHE6-GFP but not the CS-associated variants. K. Representative micrographs (left) and quantification using Pearson's correlation (right) determining fractional colocalization of NHE9 (green) with transferrin (TFN) (red) in DAPI-(blue) stained ApoE4 astrocytes following 60 minutes of uptake. Note prominent endosomal colocalization of NHE9 as evident in the merge and orthogonal slices (Z) as yellow puncta (Pearson's correlation: 0.74±0.10; $n$=40). L. Representative FACS histograms (left) and quantification of mean fluorescence intensity of biological triplicates (right) demonstrating no difference in Aβ internalization between ApoE4 (red) and ApoE4 astrocytes with NHE9-GFP expression (green). x-axis depicts Aβ clearance in logarithmic scale and vertical dashed line represents median fluorescence intensity ($p$=0.155; $n$=3; Student's $t$-test). Scale bars, 10μm. NS, Not significant.

Fig. S7

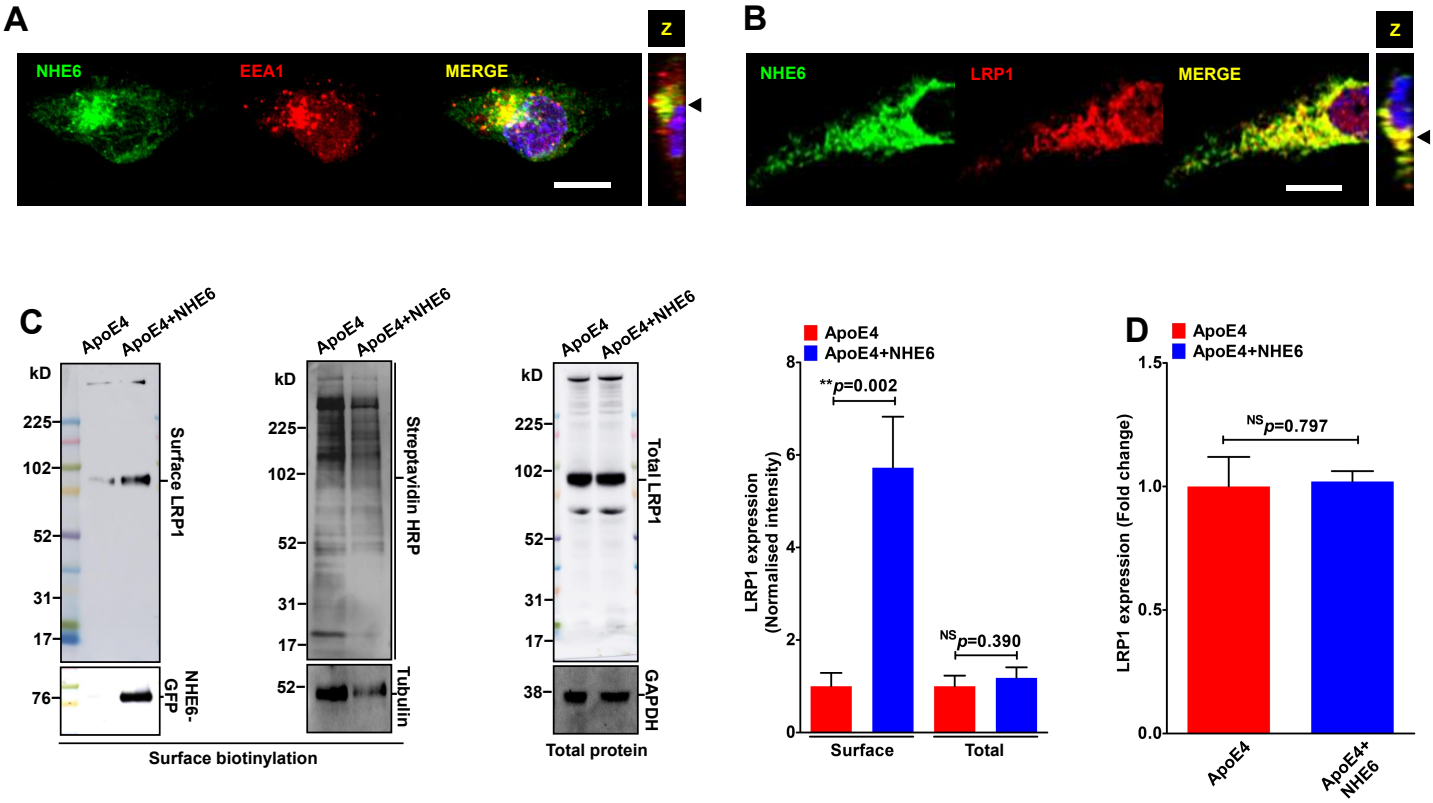
A
NHE6
EEA1
MERGE
Z
B
NHE6
LRP1
MERGE
Z
C
ApoE4
ApoE4+NHE6
kD
225
102
52
31
17
76
Surface LRP1
NHE6-GFP
Surface biotinylation
Streptavidin HRP
Tubulin
Total LRP1
GAPDH
Total protein
LRP1 expression (Normalised intensity)
**p=0.002
NSp=0.390
Surface
Total
D
LRP1 expression (Fold change)
NSp=0.797
ApoE4+ NHE6

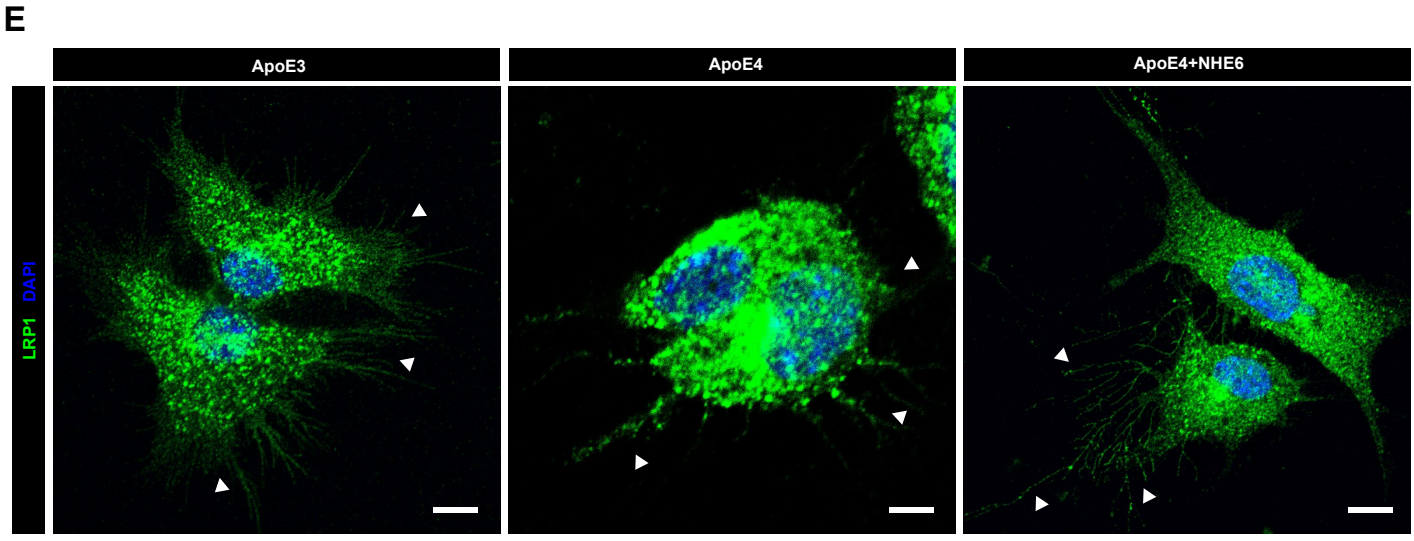
E
ApoE3
ApoE4
ApoE4+NHE6
LRP1 DAPI

**Fig. S7. NHE6 corrects defective surface LRP1 expression in ApoE4 astrocytes. Related to Fig. 4.**

(A-B) Representative immunofluorescence images of permeabilized, fixed ApoE4 astrocytes expressing NHE6-GFP showing overlap of NHE6 (green) with red-labeled EEA1 (A) and LRP1 (B). Colocalization is evident in the merge and orthogonal slices (Z) as yellow puncta. C. Representative blots showing surface (left) and total (right) LRP1 protein levels with NHE6-GFP expression (detected using anti-GFP antibody) relative to empty vector transfection. As loading control, surface biotinylated proteins were visualized with HRP-streptavidin and by probing against tubulin. GAPDH was used as a loading control for western analysis of total LRP1 levels. Quantification (extreme right) of blots showed robust ~5.7-fold higher surface LRP1 levels in ApoE4 cells with restored NHE6 expression, compared to transfection with empty vector (***p*=0.002; *n*=3; Student's *t*-test). No concomitant changes in total LRP1 levels (*p*=0.390; *n*=3; Student's *t*-test) suggesting that increased surface LRP1 was due to posttranslational redistribution of the existing cellular LRP1 pool. D. qPCR analysis confirmed no concomitant changes in LRP1 transcript with lentiviral transduction of NHE6-GFP, relative to empty vector control (*p*=0.797; *n*=3; Student's *t*-test). E. Confocal micrographs revealing a reduction in perinuclear accumulation of LRP1 (green) and partial restoration of staining on astrocyte processes (white arrow) in ApoE4 cells with NHE6 expression, similar to that observed in ApoE3 astrocytes (left). Scale bars, 10μm. NS, Not significant.

Fig. S8

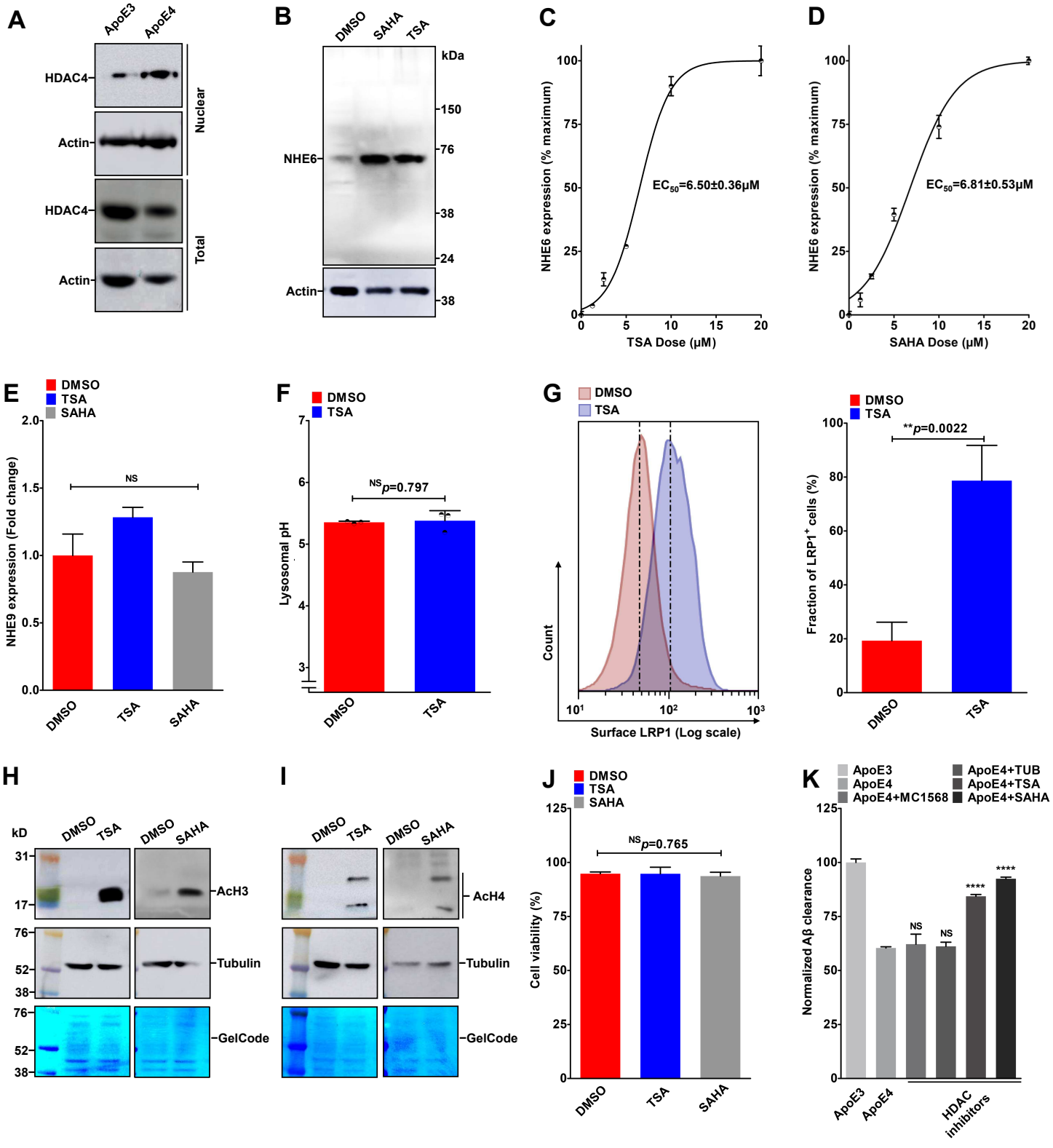
A
ApoE3
ApoE4
HDAC4
Actin
Nuclear
HDAC4
Actin
Total
B
DMSO
SAHA
TSA
kDa
NHE6
Actin
150
76
38
24
38
C
NHE6 expression (% maximum)
EC50=6.50±0.36μM
TSA Dose (μM)
D
NHE6 expression (% maximum)
EC50=6.81±0.53μM
SAHA Dose (μM)
E
DMSO
TSA
SAHA
NHE9 expression (Fold change)
NS
F
DMSO
TSA
Lysosomal pH
NS p=0.797
G
DMSO
TSA
Count
Surface LRP1 (Log scale)
DMSO
TSA
**p=0.0022
Fraction of LRP1+ cells (%)
H
kD
DMSO
TSA
DMSO
SAHA
AcH3
Tubulin
GelCode
I
DMSO
TSA
DMSO
SAHA
AcH4
Tubulin
GelCode
J
DMSO
TSA
SAHA
Cell viability (%)
NS p=0.765
K
ApoE3
ApoE4
ApoE4+MC1568
ApoE4+TUB
ApoE4+TSA
ApoE4+SAHA
Normalized Aβ clearance
NS
NS
****
****
ApoE3
ApoE4
HDAC inhibitors

**Fig. S8. HDAC inhibitors restore NHE6 levels and correct Aβ clearance deficits in ApoE4 astrocytes. Related to Fig 5.**

A. Western blot of nuclear and total fractions for HDAC4 levels in ApoE4 astrocytes relative to ApoE3. Higher HDAC4 in the nuclear fraction is suggestive of increased nuclear translocation of HDACs in ApoE4 cells. B. Western blot analysis showing robust increase of NHE6 protein with HDAC inhibition by SAHA and TSA treatment. See related Fig. 5C. (C-D) Dose response relationship to determine the potential of increasing dosage (1.25-20μM) of TSA (C) and SAHA (D) to enhance expression of NHE6 in ApoE4 astrocytes. Note characteristic sigmoidal dose-response curves with half-maximal response ($EC_{50}$) of 6.50±0.36μM and 6.81±0.53μM for TSA and SAHA, respectively. E. qPCR analysis revealed no significant changes in NHE9 expression with TSA or SAHA treatment of ApoE4 astrocytes. F. TSA treatment (5μM for 12h) did not affect lysosomal pH in ApoE4 astrocytes, relative to DMSO treatment ($p$=0.797; $n$=3; Student's $t$-test). G. Plasma membrane levels of LRP1, determined by surface labeling at 4°C and flow cytometry, are elevated in ApoE4 astrocytes with TSA treatment. x-axis in representative FACS histograms depicts surface LRP1 in logarithmic scale and vertical dashed line represents median fluorescence intensity. Quantification of percentage of $LRP1^+$ cells is shown in the right (**$p$=0.0022; $n$=3; Student's $t$-test). See related Fig. 5E. (H-I). Western blot showing acetylation of histone H3 (AcH3) (H) and histone H4 (AcH4) (I) following 60-minutes treatment with TSA and SAHA. As loading control, transferred proteins were visualized with Gelcode Blue staining and by probing against tubulin. J. TSA or SAHA treatment in ApoE4 astrocytes did not affect cell viability measured using trypan blue exclusion. K. Quantitation of measurements of Aβ clearance from FACS analysis of ApoE3 and ApoE4 cells treated with DMSO and ApoE4 cells with treatment with a panel of HDAC inhibitors. Note that broad-spectrum HDAC inhibitors (e.g. TSA and SAHA) that significantly restored NHE6 expression elicited proportionally complete correction of defective Aβ clearance in ApoE4 astrocytes to levels similar (up to 92.4%) to ApoE3 cells. HDAC inhibitors with lower induction of NHE6 expression (e.g. MC1568 and tubacin) conferred minimal changes in Aβ clearance. See related Fig. 5F. NS, Not significant.

**References**


1. Prasad H & Rao R (2015) The Na+/H+ exchanger NHE6 modulates endosomal pH to control processing of amyloid precursor protein in a cell culture model of Alzheimer disease. *The Journal of biological chemistry* 290(9):5311-5327.
2. Zhong L, *et al.* (2016) A rapid and cost-effective method for genotyping apolipoprotein E gene polymorphism. *Molecular neurodegeneration* 11:2.
3. Kondapalli KC, *et al.* (2013) Functional evaluation of autism-associated mutations in NHE9. *Nature communications* 4:2510.
4. Kondapalli KC, Prasad H, & Rao R (2014) An inside job: how endosomal Na(+)/H(+) exchangers link to autism and neurological disease. *Front Cell Neurosci* 8:172.
5. Ashkenazy H, *et al.* (2016) ConSurf 2016: an improved methodology to estimate and visualize evolutionary conservation in macromolecules. *Nucleic acids research* 44(W1):W344-350.
6. Wolfe DM, *et al.* (2013) Autophagy failure in Alzheimer's disease and the role of defective lysosomal acidification. *The European journal of neuroscience* 37(12):1949-1961.
7. Lee JH, *et al.* (2010) Lysosomal proteolysis and autophagy require presenilin 1 and are disrupted by Alzheimer-related PS1 mutations. *Cell* 141(7):1146-1158.
8. Kondapalli KC, *et al.* (2015) A leak pathway for luminal protons in endosomes drives oncogenic signalling in glioblastoma. *Nature communications* 6:6289.
9. Franck P, *et al.* (1996) Measurement of intracellular pH in cultured cells by flow cytometry with BCECF-AM. *Journal of biotechnology* 46(3):187-195.
10. Burr ML, *et al.* (2017) CMTM6 maintains the expression of PD-L1 and regulates anti-tumour immunity. *Nature* 549(7670):101-105.